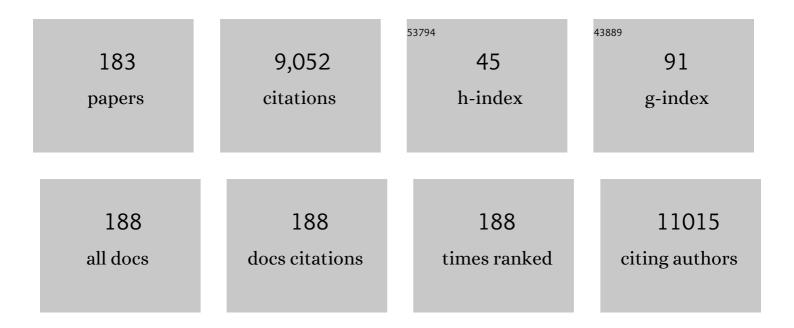
List of Publications by Year in descending order

Source: https://exaly.com/author-pdf/4424513/publications.pdf Version: 2024-02-01



#	Article	IF	CITATIONS
1	Improvement of structural quality of AlN layers grown on c-plane sapphire substrate by metal–organic vapor phase epitaxy using post-growth annealing with trimethylgallium. AIP Advances, 2022, 12, 015203.	1.3	0
2	High-mobility p-channel wide-bandgap transistors based on hydrogen-terminated diamond/hexagonal boron nitride heterostructures. Nature Electronics, 2022, 5, 37-44.	26.0	70
3	Electron transport properties in degenerate magnesium tin oxynitride (Mg _{1â^'<i>x</i>} Sn _{1+<i>x</i>} N _{2â^'2<i>y</i>} O _{2<i>y</i>}) with average wurtzite structure. Journal of Applied Physics, 2022, 131, 075302.	2.5	2
4	Synthesis of CaSnN ₂ via a High-Pressure Metathesis Reaction and the Properties of II-Sn-N ₂ (II = Ca, Mg, Zn) Semiconductors. Inorganic Chemistry, 2021, 60, 1773-1779.	4.0	18
5	Composition-Dependent Properties of Wurtzite-Type Mg _{1+<i>x</i>} Sn _{1–<i>x</i>} N ₂ Epitaxially Grown on GaN(001) Templates. ACS Applied Electronic Materials, 2021, 3, 1341-1349.	4.3	12
6	Thermal mismatch induced stress characterization by dynamic resonance based on diamond MEMS. Applied Physics Express, 2021, 14, 045501.	2.4	3
7	Temperature dependence of Young's modulus of single-crystal diamond determined by dynamic resonance. Diamond and Related Materials, 2021, 116, 108403.	3.9	17
8	Integrated TbDyFe Film on a Singleâ€Crystal Diamond Microelectromechanical Resonator for Magnetic Sensing. Physica Status Solidi - Rapid Research Letters, 2021, 15, 2100352.	2.4	2
9	The electric double layer effect and its strong suppression at Li+ solid electrolyte/hydrogenated diamond interfaces. Communications Chemistry, 2021, 4, .	4.5	15
10	Optical and electrical properties of silicon-implanted α-Al ₂ O ₃ . Japanese Journal of Applied Physics, 2021, 60, 106502.	1.5	2
11	Band Gap-Tunable (Mg, Zn)SnN ₂ Earth-Abundant Alloys with a Wurtzite Structure. ACS Applied Electronic Materials, 2021, 3, 4934-4942.	4.3	14
12	Synthesis of a Novel Rocksaltâ€Type Ternary Nitride Semiconductor MgSnN ₂ Using the Metathesis Reaction under High Pressure. European Journal of Inorganic Chemistry, 2020, 2020, 446-451.	2.0	33
13	Charge-carrier mobility in hydrogen-terminated diamond field-effect transistors. Journal of Applied Physics, 2020, 127, .	2.5	33
14	Synthesis of a Novel Rocksalt-Type Ternary Nitride Semiconductor MgSnN2 Using the Metathesis Reaction Under High Pressure. European Journal of Inorganic Chemistry, 2020, 2020, 418-418.	2.0	0
15	Precise characterization of atomic-scale corrosion of single crystal diamond in H2 plasma based on MEMS/NEMS. Corrosion Science, 2020, 170, 108651.	6.6	6
16	Photoelectron spectroscopic study of electronic states and surface structure of an in situ cleaved In2O3 (111) single crystal. Japanese Journal of Applied Physics, 2019, 58, SDDG06.	1.5	7
17	Photoelectron spectroscopic study on electronic state and electrical properties of SnO2 single crystals. Japanese Journal of Applied Physics, 2019, 58, 080903.	1.5	6
18	Optoelectronic characteristics of the Ag-doped Si p-n photodiodes prepared by a facile thermal diffusion process. AIP Advances, 2019, 9, 055024.	1.3	4

#	Article	IF	CITATIONS
19	Single-crystal diamond microelectromechanical resonator integrated with a magneto-strictive galfenol film for magnetic sensing. Carbon, 2019, 152, 788-795.	10.3	26
20	Silicon-compatible Mg2Si/Si n-p photodiodes with high room temperature infrared responsivity. Materials Science in Semiconductor Processing, 2019, 102, 104577.	4.0	12
21	Fabrication of coherent <i>γ</i> -Al ₂ O ₃ /Ga ₂ O ₃ superlattices on MgAl ₂ O ₄ substrates. Applied Physics Express, 2019, 12, 065503.	2.4	11
22	Energyâ€Efficient Metal–Insulator–Metalâ€6emiconductor Fieldâ€Effect Transistors Based on 2D Carrier Gases. Advanced Electronic Materials, 2019, 5, 1800832.	5.1	39
23	Threshold Voltage Instability of Diamond Metal–Oxide–Semiconductor Fieldâ€Effect Transistors Based on 2D Hole Gas. Physica Status Solidi (A) Applications and Materials Science, 2019, 216, 1900538.	1.8	2
24	Quantum oscillations in diamond field-effect transistors with a <mml:math xmlns:mml="http://www.w3.org/1998/Math/MathML"><mml:mi>h</mml:mi> -BN gate dielectric. Physical Review Materials, 2019, 3, .</mml:math 	2.4	16
25	A density functional study of the effect of hydrogen on electronic properties and band discontinuity at anatase TiO2/diamond interface. Journal of Applied Physics, 2018, 123, .	2.5	8
26	Annealing effects on hydrogenated diamond NOR logic circuits. Applied Physics Letters, 2018, 112, .	3.3	15
27	α-Al ₂ O ₃ /Ga ₂ O ₃ superlattices coherently grown on <i>r</i> -plane sapphire. Applied Physics Express, 2018, 11, 065501.	2.4	21
28	Direct observation of inversion capacitance in p-type diamond MOS capacitors with an electron injection layer. Japanese Journal of Applied Physics, 2018, 57, 04FR01.	1.5	14
29	Surface and bulk electronic structures of unintentionally and Mg-doped In0.7Ga0.3N epilayer by hard X-ray photoelectron spectroscopy. Journal of Applied Physics, 2018, 123, 095701.	2.5	1
30	High-mobility diamond field effect transistor with a monocrystalline h-BN gate dielectric. APL Materials, 2018, 6, .	5.1	59
31	Effect of Boron Incorporation on Structural and Optical Properties of AlN Layers Grown by Metalâ€Organic Vapor Phase Epitaxy. Physica Status Solidi (A) Applications and Materials Science, 2018, 215, 1800282.	1.8	15
32	Reducing intrinsic energy dissipation in diamond-on-diamond mechanical resonators toward one million quality factor. Physical Review Materials, 2018, 2, .	2.4	17
33	Effect of off-cut angle of hydrogen-terminated diamond(111) substrate on the quality of AlN towards high-density AlN/diamond(111) interface hole channel. Journal of Applied Physics, 2017, 121, .	2.5	16
34	Logic Circuits With Hydrogenated Diamond Field-Effect Transistors. IEEE Electron Device Letters, 2017, 38, 922-925.	3.9	49
35	Deposition of TiO2/Al2O3 bilayer on hydrogenated diamond for electronic devices: Capacitors, field-effect transistors, and logic inverters. Journal of Applied Physics, 2017, 121, .	2.5	42
36	Surface and bulk electronic structures of heavily Mg-doped InN epilayer by hard X-ray photoelectron spectroscopy. Journal of Applied Physics, 2017, 121, .	2.5	5

#	Article	IF	CITATIONS
37	Photoelectron spectroscopic study of electronic state and surface structure of In2O3 single crystals. Applied Physics Express, 2017, 10, 011102.	2.4	9
38	Effect of Sputter Deposition Atmosphere of AlN on the Electrical Properties of Hydrogenâ€Terminated Diamond Field Effect Transistor with AlN/Al ₂ O ₃ Stack Gate. Physica Status Solidi (A) Applications and Materials Science, 2017, 214, 1700463.	1.8	1
39	Reducing energy dissipation and surface effect of diamond nanoelectromechanical resonators by annealing in oxygen ambient. Carbon, 2017, 124, 281-287.	10.3	11
40	Magnetic Control of Magneto-Electrochemical Cell and Electric Double Layer Transistor. Scientific Reports, 2017, 7, 10534.	3.3	20
41	Thiourea bridged periodic mesoporous organosilica with ultra-small Pd nanoparticles for coupling reactions. RSC Advances, 2017, 7, 56306-56310.	3.6	57
42	Improvement of the quality factor of single crystal diamond mechanical resonators. Japanese Journal of Applied Physics, 2017, 56, 024101.	1.5	26
43	Nanometer-thin ALD-Al ₂ O ₃ for the improvement of the structural quality of AlN grown on sapphire substrate by MOVPE. Physica Status Solidi (A) Applications and Materials Science, 2017, 214, 1600727.	1.8	5
44	Formation Mechanism and Elimination of Smallâ€Angle Grain Boundary in AlN Grown on (0001) Sapphire Substrate. , 2017, , .		0
45	Bottom-electrode effect on switching behavior and interface reaction in nanoionic-based resistive changing memory. Japanese Journal of Applied Physics, 2016, 55, 08PC03.	1.5	1
46	Ordered Mesoporous Cobalt Phosphate with Crystallized Walls toward Highly Active Water Oxidation Electrocatalysts. Small, 2016, 12, 1709-1715.	10.0	153
47	Structural properties and transfer characteristics of sputter deposition AlN and atomic layer deposition Al2O3 bilayer gate materials for H-terminated diamond field effect transistors. Journal of Applied Physics, 2016, 120, .	2.5	22
48	Assembly of a high-dielectric constant thin TiOx layer directly on H-terminated semiconductor diamond. Applied Physics Letters, 2016, 108, .	3.3	26
49	High- <i>k</i> ZrO2/Al2O3 bilayer on hydrogenated diamond: Band configuration, breakdown field, and electrical properties of field-effect transistors. Journal of Applied Physics, 2016, 120, .	2.5	25
50	Phosphonate-Derived Nanoporous Metal Phosphates and Their Superior Energy Storage Application. ACS Applied Materials & Interfaces, 2016, 8, 9790-9797.	8.0	71
51	Superior electrocatalytic activity of mesoporous Au film templated from diblock copolymer micelles. Nano Research, 2016, 9, 1752-1762.	10.4	46
52	Electrical hysteresis in p-GaN metal–oxide–semiconductor capacitor with atomic-layer-deposited Al ₂ O ₃ as gate dielectric. Applied Physics Express, 2016, 9, 121002.	2.4	19
53	Mesoporous Pt nanospheres with designed pore surface as highly active electrocatalyst. Chemical Science, 2016, 7, 1575-1581.	7.4	197
54	Electrotactile Augmentation for Carving Guidance. IEEE Transactions on Haptics, 2016, 9, 43-53.	2.7	4

#	Article	IF	CITATIONS
55	Rücktitelbild: Polymeric Micelle Assembly with Inorganic Nanosheets for Construction of Mesoporous Architectures with Crystallized Walls (Angew. Chem. 14/2015). Angewandte Chemie, 2015, 127, 4478-4478.	2.0	0
56	Multimetallic Mesoporous Spheres Through Surfactantâ€Directed Synthesis. Advanced Science, 2015, 2, 1500112.	11.2	116
57	Mesoporous Spheres: Multimetallic Mesoporous Spheres Through Surfactant-Directed Synthesis (Adv.) Tj ETQq1	1 0,7843 11.2	14 ₁ rgBT /Ove
58	Control of normally on/off characteristics in hydrogenated diamond metal-insulator-semiconductor field-effect transistors. Journal of Applied Physics, 2015, 118, .	2.5	35
59	Influence of surface structure of (0001) sapphire substrate on the elimination of small-angle grain boundary in AlN epilayer. AIP Advances, 2015, 5, 097143.	1.3	4
60	Unobtrusive tactile sensing based on electromechanical boundary estimation. , 2015, 2015, 4375-8.		4
61	Oxygenâ€Assisted Synthesis of Mesoporous Palladium Nanoparticles as Highly Active Electrocatalysts. Chemistry - A European Journal, 2015, 21, 18671-18676.	3.3	6
62	Easy and General Synthesis of Largeâ€5ized Mesoporous Rareâ€Earth Oxide Thin Films by ′Micelle Assemblyâ€ Chemistry - an Asian Journal, 2015, 10, 2590-2593.	²² 3.3	2
63	Controlled Synthesis of Nanoporous Nickel Oxide with Twoâ€Dimensional Shapes through Thermal Decomposition of Metal–Cyanide Hybrid Coordination Polymers. Chemistry - A European Journal, 2015, 21, 3605-3612.	3.3	64
64	Thermal Conversion of Core–Shell Metal–Organic Frameworks: A New Method for Selectively Functionalized Nanoporous Hybrid Carbon. Journal of the American Chemical Society, 2015, 137, 1572-1580.	13.7	1,307
65	Dual Softâ€Template System Based on Colloidal Chemistry for the Synthesis of Hollow Mesoporous Silica Nanoparticles. Chemistry - A European Journal, 2015, 21, 6375-6380.	3.3	55
66	Shape-controlled synthesis of mesoporous iron phosphate materials with crystallized frameworks. Chemical Communications, 2015, 51, 13806-13809.	4.1	20
67	Impedance analysis of Al2O3/H-terminated diamond metal-oxide-semiconductor structures. Applied Physics Letters, 2015, 106, 083506.	3.3	16
68	A Solution Phase Synthesis of Dendritic Platinum Nanoelectrocatalysts with the Assistance of Polyoxyethylene Nonylphenyl Ether. Journal of Inorganic and Organometallic Polymers and Materials, 2015, 25, 245-250.	3.7	6
69	Bias induced Cu ion migration behavior in resistive change memory structure observed by hard X-ray photoelectron spectroscopy. Japanese Journal of Applied Physics, 2015, 54, 06FG01.	1.5	3
70	Polymeric Micelle Assembly with Inorganic Nanosheets for Construction of Mesoporous Architectures with Crystallized Walls. Angewandte Chemie - International Edition, 2015, 54, 4222-4225.	13.8	64
71	AgBiS2 single crystal grown using slow cooling method and its characterization. Journal of Crystal Growth, 2015, 411, 1-3.	1.5	15
72	Electrical properties of atomic layer deposited HfO2/Al2O3 multilayer on diamond. Diamond and Related Materials. 2015, 54, 55-58.	3.9	21

#	Article	IF	CITATIONS
73	Synthesis of a Large‧ized Mesoporous Phosphosilicate Thin Film through Evaporationâ€Induced Polymeric Micelle Assembly. Chemistry - an Asian Journal, 2015, 10, 183-187.	3.3	5
74	Sound-aided Tracing System for Visually Impaired People. Transactions of the Institute of Systems Control and Information Engineers, 2015, 28, 205-212.	0.1	0
75	Diamond FETs using heterojunction and high-k dielectrics. , 2014, , .		Ο
76	Diamond field effect transistors with a high-dielectric constant Ta ₂ O ₅ as gate material. Journal Physics D: Applied Physics, 2014, 47, 245102.	2.8	31
77	Singleâ€Crystalâ€like Nanoporous Spinel Oxides: A Strategy for Synthesis of Nanoporous Metal Oxides Utilizing Metal yanide Hybrid Coordination Polymers. Chemistry - A European Journal, 2014, 20, 17375-17384.	3.3	41
78	Diamond logic inverter with enhancement-mode metal-insulator-semiconductor field effect transistor. Applied Physics Letters, 2014, 105, .	3.3	29
79	SnS crystal grown using horizontal gradient freeze method and its electrical properties. Journal of Alloys and Compounds, 2014, 591, 326-328.	5.5	11
80	Thermal Conversion of Hollow Prussian Blue Nanoparticles into Nanoporous Iron Oxides with Crystallized Hematite Phase. European Journal of Inorganic Chemistry, 2014, 2014, 1137-1141.	2.0	27
81	Synthesis of Nanoporous Carbon–Cobaltâ€Oxide Hybrid Electrocatalysts by Thermal Conversion of Metal–Organic Frameworks. Chemistry - A European Journal, 2014, 20, 4217-4221.	3.3	253
82	Synthesis of Mesoporous TiO ₂ /SiO ₂ Hybrid Films as an Efficient Photocatalyst by Polymeric Micelle Assembly. Chemistry - A European Journal, 2014, 20, 6027-6032.	3.3	123
83	Displacement Plating of a Mesoporous Pt Skin onto Co Nanochains in a Lowâ€Concentration Surfactant Solution. Chemistry - A European Journal, 2014, 20, 3277-3282.	3.3	32
84	Mesoporous Pt hollow cubes with controlled shell thicknesses and investigation of their electrocatalytic performance. Chemical Communications, 2014, 50, 15337-15340.	4.1	62
85	Morphology development of GaN nanowires using a pulsed-mode MOCVD growth technique. CrystEngComm, 2014, 16, 2273-2282.	2.6	82
86	A universal approach to the preparation of colloidal mesoporous platinum nanoparticles with controlled particle sizes in a wide range from 20 nm to 200 nm. Physical Chemistry Chemical Physics, 2014, 16, 8787-8790.	2.8	28
87	Electric Double‣ayer Capacitors Based on Highly Graphitized Nanoporous Carbons Derived from ZIFâ€67. Chemistry - A European Journal, 2014, 20, 7895-7900.	3.3	423
88	Direct Synthesis of MOFâ€Derived Nanoporous Carbon with Magnetic Co Nanoparticles toward Efficient Water Treatment. Small, 2014, 10, 2096-2107.	10.0	588
89	Controlled Crystallization of Cyanoâ€Bridged Cu–Pt Coordination Polymers with Twoâ€Đimensional Morphology. Chemistry - an Asian Journal, 2014, 9, 1511-1514.	3.3	14
90	Low on-resistance diamond field effect transistor with high-k ZrO2 as dielectric. Scientific Reports, 2014, 4, 6395.	3.3	107

#	Article	IF	CITATIONS
91	Bolus Transport Simulation by Peristaltic Movement of Esophagus. The Japanese Journal for Medical Virtual Reality, 2014, 12, 9-14.	0.2	0
92	Interfacial electronic band alignment of Ta2O5/hydrogen-terminated diamond heterojunction determined by X-ray photoelectron spectroscopy. Diamond and Related Materials, 2013, 38, 24-27.	3.9	11
93	Allâ€Metal Mesoporous Nanocolloids: Solutionâ€Phase Synthesis of Core–Shell Pd@Pt Nanoparticles with a Designed Concave Surface. Angewandte Chemie - International Edition, 2013, 52, 13611-13615.	13.8	211
94	Electrically multiplexed tactile interface: fusion of smart tactile sensor and display. , 2013, , .		4
95	Kinetically Controlled Crystallization for Synthesis of Monodispersed Coordination Polymer Nanocubes and Their Selfâ€Assembly to Periodic Arrangements. Chemistry - A European Journal, 2013, 19, 1882-1885.	3.3	122
96	Electrical characteristics of hydrogen-terminated diamond metal-oxide-semiconductor with atomic layer deposited HfO2 as gate dielectric. Applied Physics Letters, 2013, 102, .	3.3	42
97	Facile synthesis of nanoporous carbons with controlled particle sizes by direct carbonization of monodispersed ZIF-8 crystals. Chemical Communications, 2013, 49, 2521.	4.1	474
98	Synthesis and characterization of Zn-doped mesoporous SnO2 by using thermally-stable block copolymer templates. Dalton Transactions, 2013, 42, 6366.	3.3	9
99	Synthesis of Highly Strained Mesostructured SrTiO ₃ /BaTiO ₃ Composite Films with Robust Ferroelectricity. Chemistry - A European Journal, 2013, 19, 4446-4450.	3.3	27
100	Tailored Design of Multiple Nanoarchitectures in Metal-Cyanide Hybrid Coordination Polymers. Journal of the American Chemical Society, 2013, 135, 384-391.	13.7	228
101	Interfacial band configuration and electrical properties of LaAlO3/Al2O3/hydrogenated-diamond metal-oxide-semiconductor field effect transistors. Journal of Applied Physics, 2013, 114, .	2.5	60
102	Impact of Mg concentration on energy-band-depth profile of Mg-doped InN epilayers analyzed by hard X-ray photoelectron spectroscopy. Applied Physics Letters, 2013, 103, .	3.3	8
103	Systematic investigation of surface and bulk electronic structure of undoped In-polar InN epilayers by hard X-ray photoelectron spectroscopy. Journal of Applied Physics, 2013, 114, .	2.5	17
104	Investigation of the near-surface structures of polar InN films by chemical-state-discriminated hard X-ray photoelectron diffraction. Applied Physics Letters, 2013, 102, .	3.3	8
105	Mesoporous Carbon Incorporated with In ₂ O ₃ Nanoparticles as Highâ€Performance Supercapacitors. European Journal of Inorganic Chemistry, 2013, 2013, 1109-1112.	2.0	92
106	Smart sensing of tool/tissue interaction by resistive coupling. , 2013, 2013, 628-31.		1
107	Normally-off HfO2-gated diamond field effect transistors. Applied Physics Letters, 2013, 103, .	3.3	105

108 3D simulation of platelet aggregation in cryosurgery. , 2013, 2013, 1891-4.

0

#	Article	IF	CITATIONS
109	Investigation of the Effect of Oxygen on the Near-Surface Electron Accumulation in Nonpolar m-Plane (101ì,,0) InN Film by Hard X-ray Photoelectron Spectroscopy. Japanese Journal of Applied Physics, 2013, 52, 08JD01.	1.5	2
110	Analysis of Broken Symmetry in Convergent-Beam Electron Diffraction along <112̄0 > and <11̄00 > Zone-Axes of AlN for Polarity Determination. Japanese Journal of Applied Physics, 2013, 52, 08JE15.	1.5	5
111	pH-responsive polymeric micelles with core–shell–corona architectures as intracellular anti-cancer drug carriers. Science and Technology of Advanced Materials, 2013, 14, 044402.	6.1	24
112	Interfacial chemical bonding state and band alignment of CaF2/hydrogen-terminated diamond heterojunction. Journal of Applied Physics, 2013, 113, 123706.	2.5	7
113	Development of Diamond-based Optical and Electronic Devices. Journal of Smart Processing, 2013, 2, 224-229.	0.1	Ο
114	Strong Correlation Between Oxygen Donor and Near-Surface Electron Accumulation in Undoped and Mg-Doped In-Polar InN Films. Applied Physics Express, 2012, 5, 031002.	2.4	6
115	Integration of high-dielectric constant Ta2O5 oxides on diamond for power devices. Applied Physics Letters, 2012, 101, .	3.3	41
116	Comprehensive Investigation of Single Crystal Diamond Deep-Ultraviolet Detectors. Japanese Journal of Applied Physics, 2012, 51, 090115.	1.5	43
117	Large Cs adsorption capability of nanostructured Prussian Blue particles with high accessible surface areas. Journal of Materials Chemistry, 2012, 22, 18261.	6.7	174
118	Synthesis of Superparamagnetic Nanoporous Iron Oxide Particles with Hollow Interiors by Using Prussian Blue Coordination Polymers. Chemistry of Materials, 2012, 24, 2698-2707.	6.7	163
119	Band offsets of Al2O3 and HfO2 oxides deposited by atomic layer deposition technique on hydrogenated diamond. Applied Physics Letters, 2012, 101, .	3.3	76
120	Nanoelectromechanical switch fabricated from single crystal diamond: Experiments and modeling. Diamond and Related Materials, 2012, 24, 69-73.	3.9	13
121	Synthesis of MoO3 nanotubes by thermal mesostructural transition of spherical triblock copolymer micelle templates. Chemical Communications, 2012, 48, 12091.	4.1	17
122	Development of AlN/diamond heterojunction field effect transistors. Diamond and Related Materials, 2012, 24, 206-209.	3.9	31
123	Electrochemical Design of Mesoporous Pt–Ru Alloy Films with Various Compositions toward Superior Electrocatalytic Performance. Chemistry - A European Journal, 2012, 18, 13142-13148.	3.3	26
124	Tailored Design of Architecturally Controlled Pt Nanoparticles with Huge Surface Areas toward Superior Unsupported Pt Electrocatalysts. ACS Applied Materials & Interfaces, 2012, 4, 2865-2869.	8.0	61
125	Tailored synthesis of various Au nanoarchitectures with branched shapes. CrystEngComm, 2012, 14, 7594.	2.6	29
126	Synthesis of Oliveâ€Shaped Mesoporous Platinum Nanoparticles (MPNs) with a Hardâ€Templating Method Using Mesoporous Silica (SBAâ€15). Chemistry - an Asian Journal, 2012, 7, 802-808.	3.3	29

#	Article	IF	CITATIONS
127	Facile Synthesis of Nanoporous Pt–Ru Alloy Spheres with Various Compositions toward Highly Active Electrocatalysts. Chemistry - an Asian Journal, 2012, 7, 876-880.	3.3	41
128	Comprehensive Investigation of Single Crystal Diamond Deep-Ultraviolet Detectors. Japanese Journal of Applied Physics, 2012, 51, 090115.	1.5	60
129	8D16 Surgical Preoperative Planning System with Haptic Device for Total Hip Arthroplasty The Proceedings of the Bioengineering Conference Annual Meeting of BED/JSME, 2012, 2012.24, _8D16-18D16-2	0.0	0
130	Spatially Transparent Tactile Sensor Utilizing Electromechanical Properties of Skin. Advanced Biomedical Engineering, 2012, 1, 89-97.	0.6	3
131	Mesoporous SiO ₂ and Nb ₂ O ₅ thin films with large spherical mesopores through self-assembly of diblock copolymers: unusual conversion to cuboidal mesopores by Nb ₂ O ₅ crystal growth. CrystEngComm, 2011, 13, 40-43.	2.6	25
132	Shape- and Size-Controlled Synthesis in Hard Templates: Sophisticated Chemical Reduction for Mesoporous Monocrystalline Platinum Nanoparticles. Journal of the American Chemical Society, 2011, 133, 14526-14529.	13.7	377
133	Mesoporous Co ₃ O ₄ for Low Temperature CO Oxidation: Effect of Calcination Temperatures on Their Catalytic Performance. Journal of Nanoscience and Nanotechnology, 2011, 11, 3843-3850.	0.9	14
134	Sophisticated Crystal Transformation of a Coordination Polymer into Mesoporous Monocrystalline Ti–Feâ€Based Oxide with Room‶emperature Ferromagnetic Behavior. Chemistry - an Asian Journal, 2011, 6, 3195-3199.	3.3	18
135	Demonstration of diamond field effect transistors by AlN/diamond heterostructure. Physica Status Solidi - Rapid Research Letters, 2011, 5, 125-127.	2.4	39
136	A Mesoporous γâ€Alumina Film with Vertical Mesoporosity: The Unusual Conversion from a <i>lm</i> \${ar 3}\$ <i>m</i> Mesostructure to Vertically Oriented γâ€Alumina Nanowires. Angewandte Chemie - International Edition, 2011, 50, 7410-7413.	13.8	49
137	Block-copolymer-assisted synthesis of hydroxyapatite nanoparticles with high surface area and uniform size. Science and Technology of Advanced Materials, 2011, 12, 045005.	6.1	44
138	8D-03 Force generation and bone destruction model by impact. The Proceedings of the Bioengineering Conference Annual Meeting of BED/JSME, 2011, 2010.23, 59-60.	0.0	0
139	Growth mechanism of c-axis-oriented AlN on (1 1 1) diamond substrates by metal-organic vapor phase epitaxy. Journal of Crystal Growth, 2010, 312, 1325-1328.	1.5	23
140	Growth mechanism of c-axis-oriented AlN on (0 0 1) diamond substrates by metal-organic vapor phase epitaxy. Journal of Crystal Growth, 2010, 312, 368-372.	1.5	24
141	Synthesis and characterization of highly ordered titania-alumina mixed oxide mesoporous films with high alumina content. Microporous and Mesoporous Materials, 2010, 134, 150-156.	4.4	23
142	Analysis of polar direction of AlN grown on (0001) sapphire and 6Hâ€SiC substrates by highâ€temperature metalâ€organic vapor phase epitaxy using coaxial impact collision ion scattering spectroscopy. Physica Status Solidi C: Current Topics in Solid State Physics, 2010, 7, 2365-2367.	0.8	3
143	Piezoelectric Pb(Zr0.52Ti0.48)O3 thin films on single crystal diamond: Structural, electrical, dielectric, and field-effect-transistor properties. Journal of Applied Physics, 2010, 107, 024101.	2.5	11
144	Improved ferroelectric properties of Pb(Zr0.52,Ti0.48)O3 thin film on single crystal diamond using CaF2 layer. Applied Physics Letters, 2010, 96, .	3.3	12

#	Article	IF	CITATIONS
145	Unipolar assembly of zinc oxide rods manifesting polarity-driven collective luminescence. Proceedings of the National Academy of Sciences of the United States of America, 2010, 107, 13588-13592.	7.1	44
146	Microstructure of AlN with two-domain structure on (001) diamond substrate grown by metal-organic vapor phase epitaxy. Diamond and Related Materials, 2010, 19, 131-133.	3.9	7
147	Recent developments in inorganically filled carbon nanotubes: successes and challenges. Science and Technology of Advanced Materials, 2010, 11, 054501.	6.1	48
148	Fabrication and electrical properties of SrTiO3/diamond junctions. Diamond and Related Materials, 2010, 19, 319-323.	3.9	3
149	Mechanism of photoconductivity gain and persistent photoconductivity for diamond photodetector. Diamond and Related Materials, 2010, 19, 205-207.	3.9	9
150	Integration of (PbZr0.52Ti0.48O3) on single crystal diamond as metal-ferroelectric-insulator-semiconductor capacitor. Applied Physics Letters, 2009, 94, .	3.3	17
151	Schottky photodiode using submicron thick diamond epilayer for flame sensing. Nano-Micro Letters, 2009, 1, 30-33.	27.0	12
152	Compressive properties of cartilage-like tissues repaired in vivo with scaffold-free, tissue engineered constructs. Clinical Biomechanics, 2009, 24, 110-116.	1.2	22
153	Schottky-barrier photodiode using p-diamond epilayer grown on p+-diamond substrates. Diamond and Related Materials, 2009, 18, 296-298.	3.9	14
154	Growth of highâ€quality thick AlGaN by highâ€ŧemperature metalorganic vapor phase epitaxy. Physica Status Solidi C: Current Topics in Solid State Physics, 2008, 5, 1559-1561.	0.8	7
155	Microstructure of threading dislocations caused by grain boundaries in AlN on sapphire substrates. Physica Status Solidi C: Current Topics in Solid State Physics, 2008, 5, 1582-1584.	0.8	4
156	Impact of high-temperature growth by metal-organic vapor phase epitaxy on microstructure of AlN on 6H-SiC substrates. Journal of Crystal Growth, 2008, 310, 2308-2313.	1.5	65
157	Persistent positive and transient absolute negative photoconductivity observed in diamond photodetectors. Physical Review B, 2008, 78, .	3.2	75
158	Vertical-type Schottky-barrier photodiode using p-diamond epilayer grown on heavily boron-doped p+-diamond substrate. Diamond and Related Materials, 2008, 17, 1916-1921.	3.9	7
159	AlN and AlGaN by MOVPE for UV Light Emitting Devices. Materials Science Forum, 2008, 590, 175-210.	0.3	2
160	Dislocations in AlN Epilayers Grown on Sapphire Substrate by High-Temperature Metal-Organic Vapor Phase Epitaxy. Japanese Journal of Applied Physics, 2007, 46, 1458-1462.	1.5	90
161	Submicron metal-semiconductor-metal diamond photodiodes toward improving the responsivity. Applied Physics Letters, 2007, 91, 163510.	3.3	13
162	Nitride-Based UV Lasers. Conference Proceedings - Lasers and Electro-Optics Society Annual Meeting-LEOS, 2007, , .	0.0	0

#	Article	IF	CITATIONS
163	Microstructure in nonpolar m-plane GaN and AlGaN films. Journal of Crystal Growth, 2007, 298, 288-292.	1.5	11
164	Epitaxial lateral overgrowth of AlN on trench-patterned AlN layers. Journal of Crystal Growth, 2007, 298, 257-260.	1.5	104
165	High-speed growth of AlGaN having high-crystalline quality and smooth surface by high-temperature MOVPE. Journal of Crystal Growth, 2007, 298, 215-218.	1.5	15
166	Growth of high-quality and crack free AlN layers on sapphire substrate by multi-growth mode modification. Journal of Crystal Growth, 2007, 298, 349-353.	1.5	74
167	Annihilation mechanism of threading dislocations in AlN grown by growth form modification method using V/III ratio. Journal of Crystal Growth, 2007, 300, 136-140.	1.5	66
168	Epitaxial lateral overgrowth of a-AlN layer on patterned a-AlN template by HT-MOVPE. Journal of Crystal Growth, 2007, 300, 141-144.	1.5	46
169	Microstructure of a-plane AlN grown on r-plane sapphire and on patterned AlN templates by metalorganic vapor phase epitaxy. Physica Status Solidi C: Current Topics in Solid State Physics, 2007, 4, 2528-2531.	0.8	8
170	Mg-doped high-quality AlxGa1–xN (x=0-1) grown by high-temperature metal-organic vapor phase epitaxy. Physica Status Solidi C: Current Topics in Solid State Physics, 2007, 4, 2502-2505.	0.8	20
171	Critical aspects of high temperature MOCVD growth of AlN epilayers on 6H-SiC substrates. Physica Status Solidi C: Current Topics in Solid State Physics, 2006, 3, 1392-1395.	0.8	10
172	Epitaxial lateral overgrowth of AlN layers on patterned sapphire substrates. Physica Status Solidi (A) Applications and Materials Science, 2006, 203, 1632-1635.	1.8	48
173	Microstructure of thick AlN grown on sapphire by high-temperature MOVPE. Physica Status Solidi (A) Applications and Materials Science, 2006, 203, 1626-1631.	1.8	48
174	Microstructure of nitrides grown on inclined c-plane sapphire and SiC substrate. Physica B: Condensed Matter, 2006, 376-377, 491-495.	2.7	2
175	Thermodynamic Aspects of Growth of AlGaN by High-Temperature Metal Organic Vapor Phase Epitaxy. Japanese Journal of Applied Physics, 2006, 45, 2502-2504.	1.5	26
176	High Temperature MOVPE Growth of AlxGa1â^'xN (0.2-1) Layers on Sapphire and SiC Substrates for the Fabrication Deep UV Optical Devices. Materials Research Society Symposia Proceedings, 2006, 955, 1.	0.1	2
177	Microstructure of epitaxial lateral overgrown AlN on trench-patterned AlN template by high-temperature metal-organic vapor phase epitaxy. Applied Physics Letters, 2006, 89, 221901.	3.3	79
178	High-Temperature Metal-Organic Vapor Phase Epitaxial Growth of AlN on Sapphire by Multi Transition Growth Mode Method Varying V/III Ratio. Japanese Journal of Applied Physics, 2006, 45, 8639-8643.	1.5	101
179	Flat (11ar20) GaN Thin Film on Precisely Offset-Controlled (1ar102) Sapphire Substrate. Japanese Journal of Applied Physics, 2005, 44, 7418-7420.	1.5	44
180	Group III nitrides grown on 4H-SiC (30 <ovl>3</ovl> 8) substrate by metal-organic vapor phase epitaxy. Materials Research Society Symposia Proceedings, 2004, 831, 165.	0.1	1

#	Article	IF	CITATIONS
181	Sublimation growth of AlN bulk crystals by seeded and spontaneous nucleation methods. Materials Research Society Symposia Proceedings, 2004, 831, 158.	0.1	1
182	High-quality Al0.12Ga0.88N film with low dislocation density grown on facet-controlled Al0.12Ga0.88N by MOVPE. Journal of Crystal Growth, 2004, 272, 377-380.	1.5	11
183	Ultraviolet Detectors Based on Ultraviolet–Ozone Modified Hydrogenated Diamond Surfaces. Applied Physics Express, 0, 2, 065501.	2.4	6